NUCL SCI TECH (2022) 33:129
https://doi.org/10.1007/s41365-022-01110-1

Research on manufacture technology of spherical fuel elements by dry-bag isostatic pressing

Zhen-Ming Lu[1,2] · **Wen-Ke Zhang**[1] · **Jie Zhang**[2] · **Xiang-Wen Zhou**[2] · **Kai-Hong Zhang**[2] · **Ma-Lin Liu**[2] · **Xuan-Ke Li**[1] · **Bing Liu**[2]

Received: 24 May 2022 / Revised: 16 August 2022 / Accepted: 21 August 2022 / Published online: 11 October 2022

Abstract The steady development of high-temperature gas-cooled reactors (HTRs) has increased the requirements for the production cost and quality of fuel elements. Green fuel element pressing is one of the key steps to increase the production capacity. This paper proposes a proprietary vacuum dry-bag isostatic pressing (DIP) apparatus. The structural change of the matrix graphite powder during the DIP process was examined by analyzing the density change of the matrix graphite spheres with pressure. The soft molding process was simulated using the finite element method. The dimensional changes in the spheres during the pressing, carbonization, and purification stages were explored. The performance of the fuel matrix produced by the DIP method was comprehensively examined. The fuel matrix met the technical requirements and its anisotropy was significantly reduced. The DIP method can significantly improve both the production efficiency and quality of fuel elements. This will play a key role in meeting the huge demand for fuel elements of HTRs and molten salt reactors.

Keywords Dry-bag isostatic pressing · High-temperature gas-cooled reactor (HTR) · Spherical fuel element · Finite element simulation · Soft molding

1 Introduction

The spherical fuel element production line for the high-temperature gas-cooled reactor-pebble-bed module (HTR-PM) successfully produced the first batch of fuel elements in August 2016, and began supplying products for China's demonstration HTR-PM at Shidao Bay, Shandong Province, in January 2021. HTR-PM, a commercial demonstration reactor, achieved its first criticality in September 2021, and grid-connected power generation in December of the same year. China is also planning a larger HTR. The feasibility of deploying HTR-PM600 with a 650 MW_e turbine driven by six HTR-PM reactor units is currently being studied. This means that China's HTR will face a broad space for development and open a new chapter [1, 2]. Furthermore, the fuel production technology at a larger scale is facing new challenges and should follow the development trends of higher efficiency and quality and reduced costs [3, 4].

The fuel elements employed in China's HTR are graphite spheres with a diameter of 60 mm. These are manufactured by molding pure nuclear-grade graphite powder and phenol formaldehyde resin. The fuel element consists of a fuel-comprising core with a diameter of 50 mm and a fuel-free shell with a thickness of 5 mm. The fuel-comprising core is surrounded by the fuel-free shell, and are

---

This work was supported by the National S&T Major Project (No. ZX06901).

✉ Zhen-Ming Lu
luzhenming@wust.edu.cn

✉ Bing Liu
bingliu@tsinghua.edu.cn

[1] Hubei Province Key Laboratory of Coal Conversion and New Carbon Materials, Wuhan University of Science and Technology, Wuhan 430081, China

[2] Institute of Nuclear and New Energy Technology, Collaborative Innovation Center of Advanced Nuclear Energy Technology, Tsinghua University, Beijing 100084, China

seamlessly bonded to each other to form a unit. The fuel is homogeneously distributed within the fuel-comprising core as coated particles [5]. The fuel elements should meet many cold- and hot-state requirements, e.g., proper geometrical density of the fuel matrix; good mechanical properties, thermal conductivity, and isotropy; low coefficient of thermal expansion (CTE) and Young's modulus; and high stability upon irradiation with fast neutrons.

The fuel element spheres for the HTR-PM are compressed by quasi-isostatic pressing (QIP). These achieve the physical properties required by the fuel matrix [6] using the fluid characteristics of the rubber in the rigid die under high pressure. Compared with steel die molding, the anisotropy is significantly reduced. The apparatus also has several advantages, including a compact structure, safety, and convenience. However, the QIP method can compress just one green pebble at a time, which limits the expansion of production and restrict the increase in production efficiency and reduction of production costs. The pressing process, which transforms the mixture of fuel particles and matrix graphite powder into the bulk green body, is one of the key steps in fuel element manufacturing that limits the production efficiency. The molding technology of spherical fuel elements (e.g., warm pressing with a steel die [7] and wet-bag isostatic pressing technology [8]) has been explored with varying results. In this study, the fuel matrix is produced by the dry-bag isostatic pressing (DIP) method, and its cold-state properties are investigated to enhance the comprehensive properties of the fuel elements and increase the production capacity and efficiency. This pressing technology can be adopted as an alternative to green spherical fuel pressing for production at a larger scale.

2 R&D of dry-bag isostatic pressing equipment

The vacuum DIP equipment (Fig. 1) employed in this study is a proprietary technology [9]. It primarily consists of a host machine, hydraulic system, and an electric control system. Specifically, the host machine serves as the main body of the press. The hydraulic system provides the host machine with the pressure required for pressing transmitted through the hydraulic medium. The electric control system controls the electronic devices of the equipment, which consists of the operations of the hydraulic system and host machine [9].

The core structure of the host machine consists of a hydraulic cylinder, an elastic capsule, a sealing device, and a vacuum unit. Figure 2 shows the working principle of the host machine. The open end of the elastic capsule is nested in the hydraulic cylinder body and sealed with the hydraulic cylinder. The space between the inner cavity of the hydraulic cylinder and elastic capsule is filled with the hydraulic medium, and is connected to the hydraulic system via the hydraulic pipeline. The sealing device can be moved up and down. It was adopted to fix the rubber mold, and forms a cavity with the elastic capsule to accommodate the rubber mold. The vacuum unit communicates with the cavity where the rubber mold is located through the pipeline. It removes the gas from the matrix powders during pressing to prevent the breakdown or internal cracking of the fuel element matrix owing to the expansion of the internal gas in the pressure-relief process.

Fig. 1 Dry-bag isostatic pressing equipment

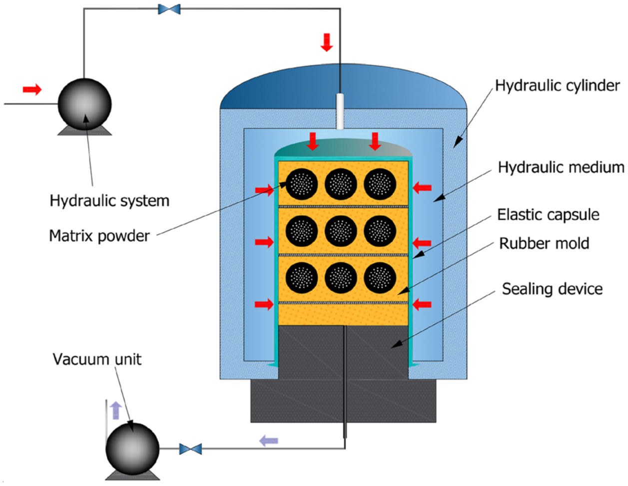

Fig. 2 Schematic diagram of the principle of DIP

For convenience and cleaning, the system isolates and transmits the pressure between the rubber mold and hydraulic medium through the elastic capsule. The soft rubber mold used was stacked into multiple layers with several cavities to charge the matrix graphite powder and nuclear fuel mixture, and distribute it evenly in each layer. The number of stacked layers and cavities can be designed according to the needs of products. The silicone rubber mold used in this experiment was independently developed. It was stacked into three layers, with nine spherical cavities in each layer. One cavity is located in the center, while the other eight are evenly distributed along the axis the mold; that is, a total of 27 fuel elements can be pressed at a time.

During the operation of the equipment, the sealing device first rises and seals the cavity with the elastic capsule. Then, the air in the matrix powder and gaps in the mold is discharged by the vacuum system. Finally, the hydraulic medium evenly transmits the pressure to the elastic capsule from all directions, and then to the rubber mold through the capsule. Under high pressure, the soft rubber mold shrinks and deforms, and transfers the pressure to the matrix powder. The matrix powder is pressed into a spherical shape under pressure from all sides.

The equipment can switch between low and high pressure working states. The low-pressure state is used to premold the core, which consists of graphite and overcoated particles with a lower density. The high pressure state is employed to apply pressure to the dense green pebbles. The DIP combines the advantages of the clean working conditions of the QIP method, and the uniform pressure and large production capacity of the wet-bag isostatic pressing method, to significantly increase the production efficiency while facilitating the realization of automated production.

3 Experiment and performance characterization

The graphite fuel matrix occupies more than 90% of the volume of the spherical fuel element while representing its structural substance. In other words, the essential properties required by the fuel element in the reactor are borne by the graphite matrix. Accordingly, to prevent fuel particles from affecting the sampling and performance test results when studying the cold-state properties of the matrix materials of fuel elements, the graphite matrix samples produced using a similar fuel element fabrication method were employed as the research target. In this study, the feasibility of preparing fuel elements by DIP was verified based on the structural changes that occur during the manufacturing of matrix graphite spheres and the comprehensive evaluation of matrix properties.

Considering the particularity of nuclear materials, pseudo-particles were employed as the nuclear fuel when preparing the element sphere, i.e., ZrO_2 particles were used as surrogates for UO_2 kernels in the TRISO particles owing to their chemical stability during heat treatment in the fuel element fabrication process and high density similar to that of UO_2 kernels. The nuclear fuel elements are thereinafter referred to as pseudo-elements.

3.1 Sample preparation

The preparation of the matrix graphite sphere and pseudo-element samples includes matrix graphite powder production, pseudo-overcoated-particle preparation, and green pebble pressing, machining, carbonization, and purification.

The matrix powder was produced through several processes (e.g., homogeneous mixing of aggregates, kneading with phenol formaldehyde resin solution, granulating with the extrusion method, removing ethanol in vacuum, crushing, and sieving) with natural flake graphite powder, synthetic graphite powder, and phenol formaldehyde resin as the main raw materials.

To obtain the pseudo-overcoated-particles, the coated ZrO_2 particles were overcoated with the matrix graphite powder at a thickness of approximately 0.2 mm using an overcoating machine.

The production process of spherical fuel elements includes premolding to prepare the fuel-containing cores and final molding to obtain the green fuel pebbles. First, a mixture of graphite molding powder and pseudo-overcoated-particles was loaded into the cavity of the stacked rubber molds layer-by-layer and precompressed into manageable sphere cores at a pressure below 10 MPa. Overcoated particles were not added during the preparation of the matrix graphite spheres. Notably, the surface of the premolded spherical core was grooved rather than smooth, which enhances the combination of the fuel-containing core and fuel-free shell. The grooves were obtained by appropriately designing the cavity, which in turn was produced while casting the rubber mold in the suitable casting matrix.

Subsequently, the premolded sphere core was embedded into the graphite molding powder in a second stacked rubber mold. The air in the powders and gaps between the soft mold and elastic capsule was exhausted by the vacuum pump. The matrix powder was pressed into green pebbles with the desired density in the final molding process. To study the formation mechanism of the matrix powder under DIP conditions, molding was performed at 50, 90, 120, 150, 210, 230, 250, and 280 MPa, respectively.

After pressing, the matrix graphite spheres or spherical fuel elements were initially heated to 800 °C for 20 h under a predetermined temperature program; held for 1 h in an inert gas to carbonize the binder [10]; and then heated in vacuum at 1900 °C for 1 h to remove metal impurities after machining into a 60 mm diameter sphere.

The green balls compressed by eight cavities of the outer loop of the rubber mold were used as the research object to ensure comparability.

3.2 Performance characterization

The performance of the matrix spheres produced using the DIP method was examined in compliance with the quality control rules for the matrix graphite spheres. The characterization methods [11] are listed in Table 1.

The equipment employed in performance testing are elucidated below:

The thermal conductivity of the graphite matrix was measured by a NETSZCH LFA 457 laser thermal conductivity meter.

The CTE of the graphite matrix was measured by a NETSZCH DIL 402CD thermal dilatometer.

The crushing load of the matrix graphite spheres was measured using a SHIMADZU AG-X100 universal testing machine.

The falling strength of the matrix graphite spheres was examined using the special device. The graphite spheres were dropped from a height of 4 m to the pebble bed to and fro.

The corrosion rate of the matrix graphite spheres was examined with the special corrosion furnace in a gas ambience of 99 vol% helium and 1 vol% water vapor at 1000 °C for 10 h.

The wear rate of the matrix graphite spheres was examined with the special device by placing 20 spheres in a cylinder chamber that was rotated for 100 h.

4 Results and analysis

4.1 Pressing characteristic curve

Figure 3 shows the change in the density of the green matrix spheres molded by DIP under pressure. To fit the P–ρ characteristic curve, the geometrical density of the matrix graphite powder, charging tap density, and density of the premolded sphere core were employed as the density data under a lower pressure.

In accordance with the equation for the fitted curve in Fig. 3, combined with the dimensions and experimental data, the pressing characteristic equation of the matrix graphite powder under the DIP condition is expressed as

$$\rho = \rho_c + \frac{\rho_0 - \rho_c}{1 + \left(P/a\right)^b}, \tag{1}$$

where ρ_c denotes the density of the spheroid in the compact state, ρ_0 is the apparent density of the matrix graphite powder, and a and b are the characteristic constants.

By taking the logarithm of Eq. (1) after shifting the terms, we obtain

$$\ln \frac{\rho_c - \rho}{\rho_c - \rho_0} = b \ln P - b \ln a. \tag{2}$$

Equation (2) is highly similar to the classical Huang Peiyun double-logarithm pressing equation [12]· The coefficients of determination R^2 and adjusted-R^2 in this model are 0.99882 and 0.99838, respectively. These values are close to 1, indicating the high goodness-of-fit of the equation model obtained by regression fitting. The pressing process can be divided into three stages in accordance with the traditional powder metallurgy theory [13] to explain the changes in the matrix graphite powder during the process.

In stage I, the rubber mold was compressed by an external hydraulic pressure. The mold cavity shrunk and deformed, causing the displacement of the matrix graphite powder particles. The interspace between the particles formed by the "arch bridge effect" was broken; the particles filled each other's pores; the positions of the powder particles were rearranged; and the contact surface area

Table 1 Performance characterization methods of the graphitic matrix spheres

Characterization items	Method
Density (g cm^{-3})	Weighing and diameter measurement
Crushing load (kN)	Pressing
Thermal conductivity (W m^{-1} K^{-1})	Laser thermal conductivity instrument
Falling strength (number of times)	Free dropping
Wear rate (mg h^{-1})	Wearing and weighing
Corrosion rate(mg cm^{-2} h^{-1})	Corroding and weighing
CTE anisotropy ($\alpha_\perp/\alpha_\|$)[a]	Thermal expansion test

[a] Parallel and perpendicular to the mold joint

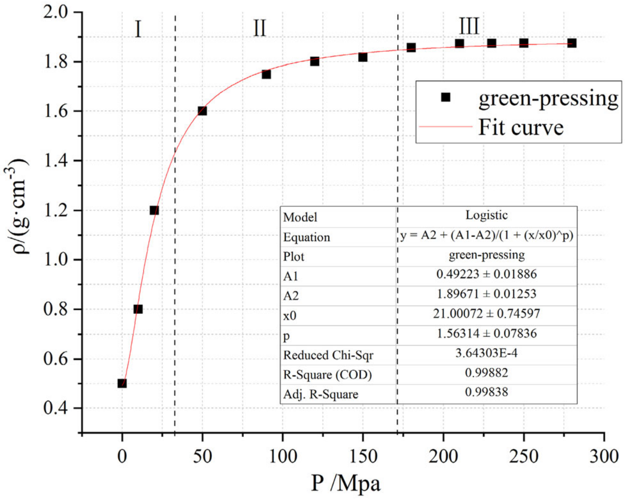

Model	Logistic
Equation	y = A2 + (A1-A2)/(1 + (x/x0)^p)
Plot	green-pressing
A1	0.49223 ± 0.01886
A2	1.89671 ± 0.01253
x0	21.00072 ± 0.74597
p	1.56314 ± 0.07836
Reduced Chi-Sqr	3.64303E-4
R-Square (COD)	0.99882
Adj. R-Square	0.99838

Fig. 3 *P*–*ρ* characteristic curve

increased. At this stage, the force required to overcome powder deformation was small; hence, the powder density in the mold cavity rapidly increased with increasing pressure. The meshing force between the powder particles was small and insufficient to press the powder into blocks.

In stage II, the interspaces between powders were filled with each other, which restricted the movement of the matrix powder particles, whereas multiple adjacent powder particles still had gaps in the three-dimensional space. When further pressurized, the matrix powder particles deformed and were further filled. Graphite is a brittle material. For brittle materials, the curve at this stage should be flat or even a plateau [13], whereas the curve in Fig. 3 does not show an inflection point. This result is attributed the layer of phenolic resin wrapped around the matrix graphite powder particles; hence, the matrix powder showed a certain plasticity. However, the density growth rate of the green matrix pebbles gradually slowed down as the pressure increased owing to the large external force required for particle deformation. At this stage, the mechanical strength of the green pebbles increased significantly with pressure. On the one hand, the interaction force between particles increased with the diversification of meshing forms and the increase in meshing interfaces between particles. However, the extrusion and relative movement between particles under high pressure produced a strong frictional force at the particle interface. The heat generated by friction softened the thermoplastic resin around the surface of the graphite particles, which acted as a binder to increase the attractive force between resin atoms, thus increasing the strength of the green pebbles.

In stage III, the matrix powder particles meshed and supported each other through deformation after going through stage II. The contact area at the interface between them was large. Consequently, the remaining tiny pores on the surface and inside the particles were difficult to eliminate. When the pressure was further increased, the increase in density was dependent on particle fragmentation to reduce the porosity, which required a larger external force; therefore, the increase in density was limited.

Figure 4 presents the density change of the matrix graphite spheres before and after heat treatment at 90–280 MPa. It can be seen that the density of the green-pressed, carbonized, and purified matrix graphite spheres changed significantly with the pressure in the range of 90–230 MPa; the change was insignificant at 230–280 MPa. In manufacturing spherical fuel elements, the appropriate pressing pressure is required to obtain the desired density and mechanical properties of the green pebbles while preventing damage to the coated particles inside the fuel element due to excessive pressure. The pressing condition of the sample element below is 280 MPa.

4.2 Simulation of pressing process

The finite element simulation method has been widely used in the compaction and sintering processes of different metals in the field of powder metallurgy [14–17]. The method analyzes not only the relationship between the overall and local relative density and compaction pressure, but also the stress distribution and powder displacement in the compact upon compaction at a macro-continuous scale. In this study, finite element simulation was carried out to analyze the matrix graphite powder compaction in a multilayer stacking mold by DIP, and the stress distribution of the rubber mold and green pebbles under high pressure.

The finite element model is illustrated in Fig. 5. The three-layer nine-ball model has a total of 751,968 cells, with each layer divided into 250,656 cells.

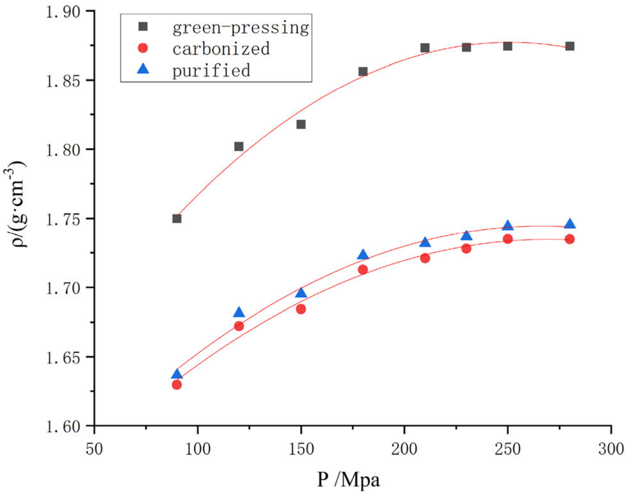

Fig. 4 Density of matrix graphite spheres at 90–280 MPa

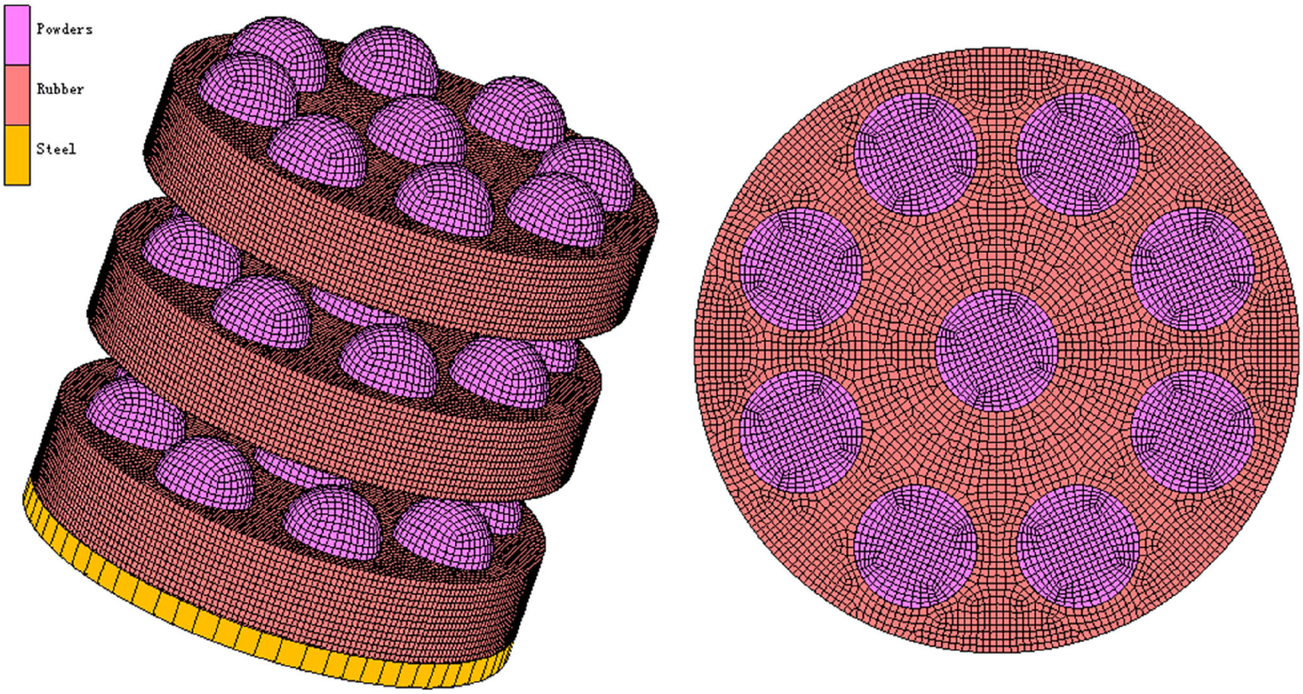

Fig. 5 The finite element model of three-layer nine-ball DIP

In finite element modeling, the graphite powder was set as a compressible continuum. The constitutive equation is the Shima–Oyane model [18, 19].

$$F = \frac{1}{\gamma}\left(\frac{3}{2}\sigma^{\mathrm{d}}\sigma^{\mathrm{d}} + \frac{\sigma_{\mathrm{m}}^2}{\beta^2}\right)^{0.5} - \sigma_{\mathrm{y}}, \tag{3}$$

where σ_{y}, σ^{d}, and σ_{m} denote the uniaxial yield stress, deviatoric stress tensor, and hydrostatic pressure, respectively; and γ and β are the material parameters fitted through the compression test.

The rubber material of the soft mold is defined by the Mooney–Rivlin model [20, 21]. The strain energy potential W can be written as

$$W = C_{10}(\bar{I}_1 - 3) + C_{01}(\bar{I}_2 - 3) + \frac{1}{d}(J - 1)^2, \tag{4}$$

where W denotes the strain energy potential; $\bar{I}_1$ and $\bar{I}_2$ are the first and second invariants of the deviatoric strain, respectively; d is the incompressibility parameter of the material; J is the elastic volume ratio; and C_{10} and C_{01} are constants fitted by the tensile test.

In the simulation process, according to the hydraulic pressure characteristics, the pressure was uniformly loaded onto the exterior surfaces of the stacked rubber mold (except the bottom) by the elastic capsule, and then transmitted to the powder in the mold cavity via the rubber mold. Figure 6 shows the radial and axial cross sections of the stress distribution in the layers of the rubber mold. As seen in the figure, the stress distributions in the three layers of the rubber mold and the matrix spheres are basically the same. The stresses of the mold between the upper and lower adjacent graphite spheres were not distinct. Overall, each ball was practically surrounded by the blue domain of the rubber mold, which indicates that the pressure from the hydraulic press was homogeneously transmitted to each matrix sphere via the rubber mold and elastic capsule [22].

Figure 7 shows a cloud diagram of the changes in the relative density distribution of the spherical compacts as the pressure increased from 0 to 280 MPa within 10 s. It can be seen that as the pressing pressure increased, the relative density of the matrix spheres in the model increased. No significant difference was observed between 252 and 280 MPa, which consistent with the above results. Furthermore, the relative density distributions in the matrix spheres under all pressures were relatively uniform.

4.3 Changes of geometric dimension

The green matrix graphite spheres underwent structural and chemical changes with the process conditions during compression molding and subsequent heat treatments (i.e., carbonization and purification). Graphite exhibits an obvious anisotropy, which has a corresponding performance in the respective process step. Specifically, the changes in geometric dimensions in different directions during the matrix pebble production process is of great concern, and plays a key role in guiding the process design [10, 23].

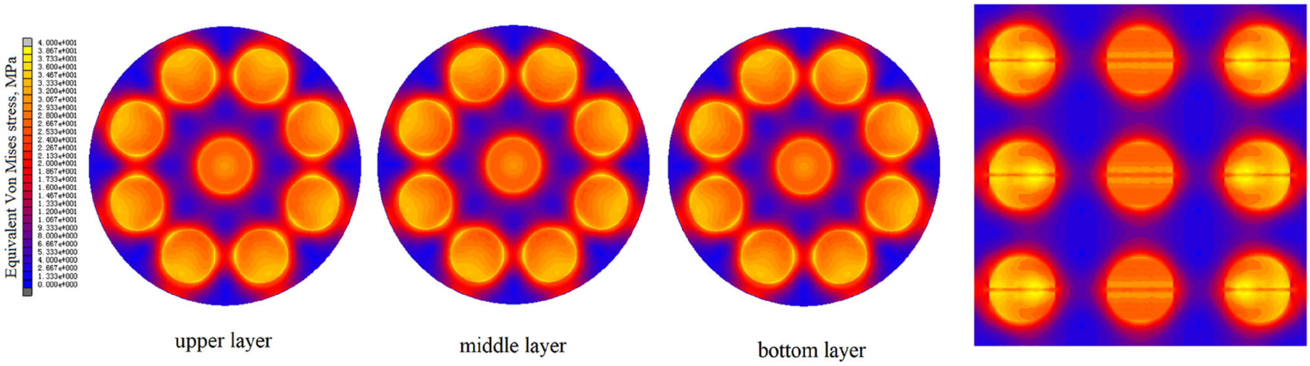

Fig. 6 Stress distribution in the rubber mold by finite element simulation

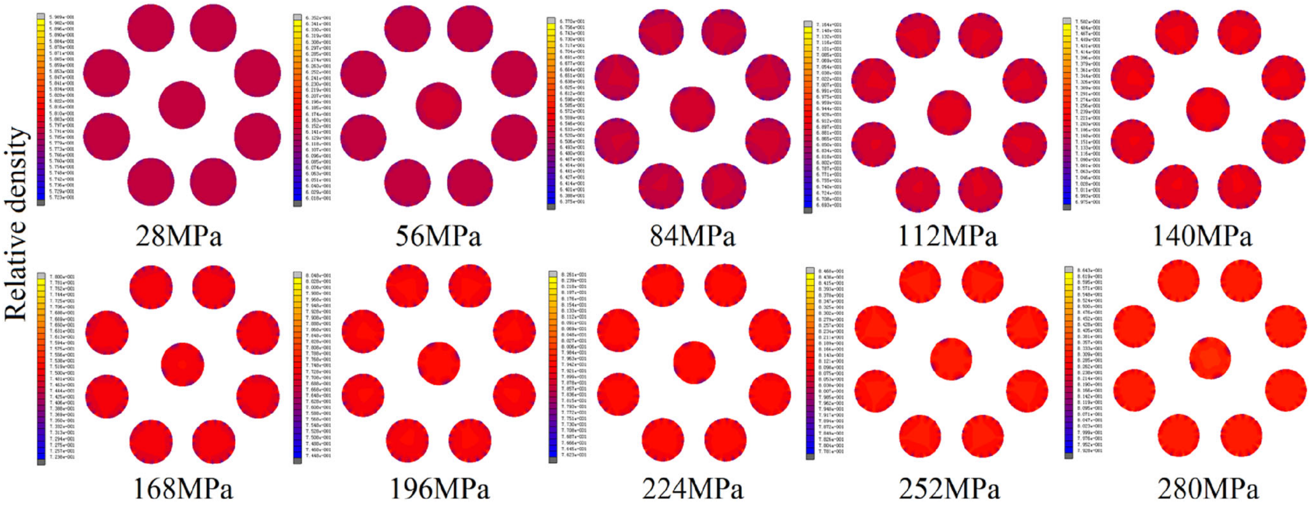

Fig. 7 Cloud diagram of the relative density distribution under different pressure

To facilitate the study of the dimensional change of the matrix sphere in different process stages, the deformation rate δ is defined as

$$\delta = [\Delta d / d_i] \times 100\%, \tag{5}$$

where d_i denotes the initial diameter of the sphere preprocessed in the corresponding step, i.e., in the pressing step, it represents the dimensions of the mold cavity; Δd represents the change in the sphere diameter before and after the corresponding step.

Ten green pebbles were randomly chosen as study objects to track the dimensional changes in the equatorial plane direction (indicated by ||) and polar direction (indicated by ⊥) during pressing, carbonization, and purification.

Figure 8 shows the dimensional change rate results. In the pressing step, the deformation rates in the ⊥- and ||-directions were measured as approximately 27% and 25%, respectively. The ratio of the mean value (MV in Fig. 8) was 1.07. In the carbonization step, the average deformation rates in the two directions were 1.44% and 1.16%, respectively, and the ratio of the MV was 1.24. In the purification step, the average deformation rates in the two directions were 0.33% and 0.29%, respectively, and the ratio of the MV was 1.13.

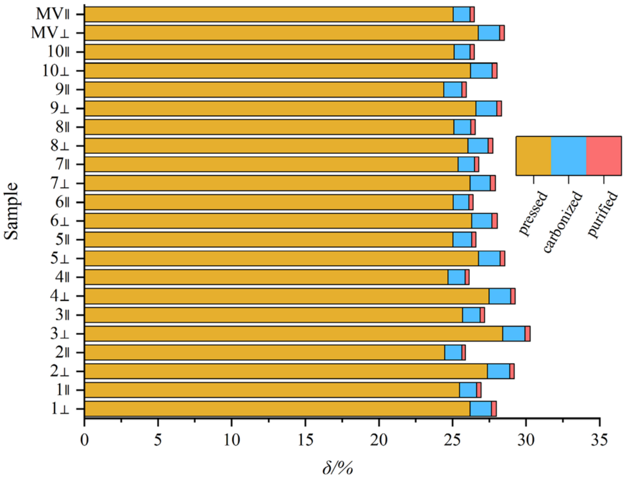

Fig. 8 Deformation rate of matrix graphite spheres in different steps

The deformation during the pressing step occurred from the loose powder to the compact spheres; therefore, the deformation rate was relatively high.

Because of the effects of various factors such as thermal expansion, chemical reactions, and crystal structure changes, the volume of the green pebbles first increased and then decreased during the carbonization process. In the initial stage, the phenol formaldehyde resin in the green matrix spheres was softened and paralyzed into light-component gases, resulting in the formation of gas channels and significant volume expansion. In the latter stage, the polycondensation of the phenol formaldehyde resin and the reconstruction and regularization of the carbon structure led to the predominance of volume shrinkage [10, 23].

In the purification step, hydrogen was released by the destruction of C-H bonds in the six-membered ring at the initial stage. The maximum purification temperature was 1900 °C. The lattice structure of the resin carbon was further regularized at this temperature, leading to shrinkage.

As revealed by the deformation rates in the three process steps of pressing, carbonization, and purification in Fig. 8, the graphite matrix showed obvious differences in the ||- and ⊥-directions. The difference between the deformation rates in the two directions at the respective step was much smaller compared with that of the QIP method used in the HTR-PM [22].

The differences between the results above in different directions are directly related to the microstructure of the fuel matrix. On the one hand, microstructural differences arose from the inherent properties of graphite materials [24], i.e., atomic structure difference between the hexagonal crystal structures of graphite crystals in the *a*- and *c*-axis directions, and the flake-like or rod-like anisotropic structures of the powder. The graphite powder with this structure exhibited an obvious preferred orientation under the action of gravity, which was attributed to the use of the pressing method. During pressing, the pressure distributions of the cylindrical dry-bag mold differed in the axial and radial directions. However, because the hydraulic pressure acted homogenously on all surfaces except the bottom of the rubber mold, the differences in the two directions were significantly reduced compared with those in the steel die pressing and QIP [5] methods, and the effect on anisotropy was much smaller.

4.4 Change of mechanical properties

Matrix graphite spheres pressed at 210, 230, 250, and 280 MPa were selected to examine the crushing load and Young's modulus, as shown in Fig. 9. The Young's modulus was derived from the simultaneous results of the crushing load examination and obtained through data conversion. As seen in the figure, the crushing load of the matrix pebble did not change significantly when the pressure exceeded 230 MPa, while the Young's modulus maintained an upward trend. In other words, the Young's modulus is more sensitive to changes in the material microstructure than the crushing load. The greater the pressure, the fewer the internal pores, and the smaller the strain under the same stress; hence, the modulus is larger. The stability of the crushing load at pressures over 230 MPa indicates that the crushing strength of the graphite matrix is not dependent on the meshing of powder particles, but is determined by the resin carbon structure formed after the carbonization of the phenol formaldehyde resin.

Figure 9 also shows that the Young's modulus is larger in the ||-direction, while the crushing loads are smaller. Although isostatic pressing was adopted, the mechanical properties of the graphite matrix showed significant anisotropy, which is inseparable from the anisotropy of the graphite powder.

4.5 Comprehensive performance evaluation

Table 2 lists the performances of the matrix graphite spheres manufactured by DIP. The comparison between the technical specifications and results indicate that all the properties meet the technical requirements. The table also summarizes the performance of the matrix pebbles compressed by the QIP method at Tsinghua University's Institute of Nuclear and New Energy Technology (INET) and the Arbeitsgemeinschaft Versuchs Reaktor (AVR) reactor [25] in Germany, respectively. The QIP technology used by the INET is the same as that used to manufacture

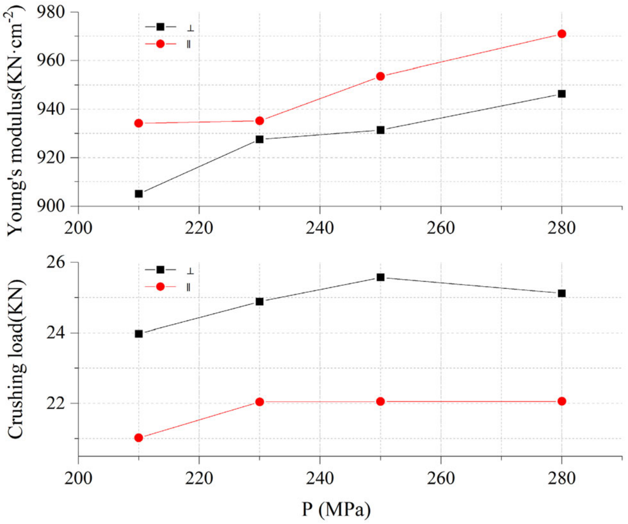

Fig. 9 Crushing load and Young's modulus of graphite balls with different pressures

Table 2 Properties comparison of prepared matrix graphite

Inspection items	Dry-bag isostatic	Quasi-isostatic		Specification
		INET	AVR-THTR	
Geometrical density (g cm^{-3})	1.75	1.74	1.73	> 1.70
Crushing load (kN)				
∥	21.86	21.20	–	≥ 18
⊥	23.77	26.36	–	
Young's modulus (kN cm^{-2})				
∥	971	976	1000	–
⊥	946	934	970	
Thermal conductivity (W m^{-1} K^{-1})				
∥	37.41	38. 49	41	≥ 25
⊥	35.57	33.68	37	
CTE (10^{-6} m K^{-1})				
∥	3.42	3.38	2.89	–
⊥	3.48	3.63	3.45	
Anisotropy ($\alpha_{\perp}/\alpha_{\parallel}$)	1.02	1.07	1.19	≤ 1.3
Corrosion rate (mg cm^{-2} h^{-1})	1.05	1.02	0.97	≤ 1.3
Wear rate (mg h^{-1})	2.01	1.81	/	≤ 6
Falling strength (number of drops)	≫ 100	≫ 100	437	≥ 50

the HTR-PM elements. The raw materials of the matrix powder are the same as those used in this study. The comparison of the results of the three methods showed no significant difference in the performance of indicators such as the density, corrosion, wear, thermal conduction, and CTE. However, for the anisotropy of CTE, the anisotropy of the matrix pebbles produced by the DIP method was significantly lower than those pressed by the QIP method. For the other indexes related to anisotropy (e.g., crushing load, modulus, and thermal conduction), the difference between the ∥- and ⊥-directions of matrix spheres molded by the DIP method was also significantly lower than those of the QIP method.

The anisotropy of the fuel matrix is related to the structure of the raw materials and compression method. During the processes of matrix powder loading into the mold cavity and green pebble compression, the flake-like or rod-shaped graphite powder particles tended to incline toward the equator of the sphere. This preferred orientation of the microstructure led to the anisotropy of macroscopic properties. However, in the DIP process, each green pebble in the soft mold cavity was independent of the isostatic pressing environment. The pressure around the pebbles was almost equal in all directions, which reduced the microstructure difference of the fuel matrix in different directions.

The spherical fuel elements in the reactor were simultaneously subjected to the thermal stress caused by the inside-out temperature gradient and the irradiation stress caused by the outside-in neutron fluence gradient [25]. The spherical fuel element compressed by the DIP method has a low anisotropy, which is beneficial for reducing the internal stress caused by the thermal and neutron fields, and further enhances the reliability of the HTR.

Crushing load is one of the most critical mechanical properties of fuel elements. The crushing load performance of the pseudo-elements prepared by the same process was examined in this study. The crushing loads in the ⊥- and ∥-directions exceeded the 18 kN required by the technical specifications for matrix graphite. Figure 10 shows the typical failure form of the element after the crushing load test. It can be seen that the failure section penetrated the interior of the element without cracking from the interface between the fuel-free shell and fuel-comprising core. This suggests that the matrix of the fuel-comprising area and fuel-free area are tightly and firmly integrated and their properties are consistent, thus ensuring the mechanical properties of the fuel element.

5 Conclusion

1. Matrix graphite spheres and spherical fuel elements were produced by the DIP method by pressing in a vacuum and the heat treatments of carbonization and purification. The results show that the performance of all cold-state properties met the technical requirements.
2. The self-developed vacuum DIP method is effective for manufacturing spherical fuel elements. The

Fig. 10 Cracked pseudo-element after crushing load test

technology can accommodate the further increase in production capacity by enlarging the mold and increasing the number of cavities in the respective layer. Increasing the number of stacking layers will significantly increase the number of green pebbles that can be pressed at one time. The DIP apparatus has a compact structure and is easy to operate. It can be connected to upstream and downstream equipment through automatic control to realize large-scale assembly line operations.

3. The anisotropy of the matrix pebbles produced by the DIP method was reflected in each process step; however, it was significantly reduced compared with that of the QIP method, which reduced the thermal stress and irradiation stress of fuel elements during the operation of the reactor [22, 26].
4. The DIP technology significantly improved both the production efficiency and quality of fuel elements. This indicates its key role in meeting the huge demand for fuel elements of HTRs and molten salt reactors [27, 28] in recent years.

Acknowledgements We thank Prof. Xi-Zhong An for his assistance with the numerical simulation and Prof. Chun-He Tang, Jiang-Hua Li, Lei Wang, Jing Song, and Shi-Fu Liu for their technical assistance.

Author contributions All authors contributed to the study conception and design. Material preparation, data collection and analysis were performed by Zhen-Ming Lu, Wen-Ke Zhang, Jie Zhang, Kai-Hong Zhang and Ma-Lin Liu. The first draft of the manuscript was written by Zhen-Ming Lu, and all authors commented on previous versions of the manuscript. All authors read and approved the final manuscript.

References

1. Z.Y. Zhang, Z.X. Wu, D.Z. Wang et al., Current status and technical description of Chinese 2×250 MW_{th} HTR-PM demonstration plant. Nucl. Eng. Des. **239**(7), 1212–1219 (2009). https://doi.org/10.1016/j.nucengdes.2009.02.023
2. Z.Y. Zhang, Y.J. Dong, F. Li et al., The Shandong Shidao bay 200 MWe high-temperature gas-cooled reactor pebble-bed module (HTR-PM) demonstration power plant: an engineering and technological innovation. Engineering **2**(1), 112–118 (2016). https://doi.org/10.1016/J.ENG.2016.01.020
3. Z.Y. Zhang, Y.J. Dong, Q. Shi et al., 600 MW_e high temperature gas-cooled reactor nuclear power plant HTR-PM600. Nucl. Sci. Tech. **33**, 101 (2022). https://doi.org/10.1007/s41365-022-01089-9
4. D. She, B. Xia, J. Guo et al., Prediction calculations for the first criticality of the HTR-PM using the PANGU code. Nucl. Sci. Tech. **32**, 90 (2021). https://doi.org/10.1007/s41365-021-00936-5
5. C.H. Tang, Y.P. Tang, J.G. Zhu et al., Design and manufacture of the fuel element for the 10 MW high temperature gas-cooled reactor. Nucl. Eng. Des. **218**, 91–102 (2002). https://doi.org/10.1016/S0029-5493(02)00201-7
6. J. Zhang, Z.M. Lu, B. Liu et al., Quasi-isostatic vacuum hydraulic press. CN Patent 201210177503.7, 31 May 2012.
7. W. Dell, R.E. Schulze, L. Blinkele et al., Warm-Moudle de graphitic matrix for spherical HTR fuel elements in Germany, Juel-Con-52, Juni, 15–19 (1985).
8. J. Zhang, B. Liu, Z.M. Lu et al., A manufacturing method of green spherical fuel element. CN Patent 201811619914.0, 28 December 2018.
9. Z.M. Lu, J. Zhang, B. Liu et al., A device and a method for pressing green spherical fuel element. CN Patent 201810509223.9, 24 May 2018
10. Z.M. Lu, J. Zhang, X.W. Zhou et al., Optimization of carbonization process in manufacture of fuel elements for HTGR. Nucl. Power. Eng. **34**(5), 71–75 (2013). (**in Chinese**)
11. H.S. Zhao, T.X. Liang, J. Zhang et al., Manufacture and characteristics of spherical fuel elements for the HTR-10. Nucl. Eng. Des. **236**, 643–647 (2006). https://doi.org/10.1016/j.nucengdes.2005.10.023
12. C.Y. Wu, L.Y. Zhang, *Mechanical Principle of Powder Forming*, 1st edn. (Metallurgical Industry Press, Beijing, 2003), pp.36–44
13. P.Y. Huang, *Principles of Powder Metallurgy*, 2nd edn. (Metallurgical Industry Press, Beijing, 1997), pp.169–189
14. X.Z. An, Y.L. Zhang, Y.X. Zhang et al., Finite element modelling on the compaction of copper powder under different conditions. Metall. Mater. Trans. A. **46**, 3744–3752 (2015). https://doi.org/10.1007/s11661-015-2929-x
15. H.Q. Fan, C.C. Huang, X. Wang et al., Numerical simulation of stress behavior of dowel–brick structures in TMSR. Nucl. Sci. Tech. **31**, 51 (2020). https://doi.org/10.1007/s41365-020-00761-2
16. Y. Zou, X.Z. An, Q. Jia et al., Three-dimensional MPFEM modelling on isostatic pressing and solid phase sintering of tungsten powders. Powder Technol. **354**, 854–866 (2019). https://doi.org/10.1016/j.powtec.2019.07.013
17. P. Han, X.Z. An, D.F. Wang et al., MPFEM simulation of compaction densification behavior of Fe-Al composite powders with different size ratios. J. Alloys Compd. **741**(15), 473–481 (2018). https://doi.org/10.1016/j.jallcom.2018.01.198
18. S. Shima, M. Oyane, Plasticity theory for porous metals. Int. J. Mech. Sci. **18**(6), 285–291 (1976). https://doi.org/10.1016/0020-7403(76)90030-8
19. S. Shima, M. Yamada, Compaction of metal powder by rolling. Powder. Metall. **27**(1), 39–44 (1984). https://doi.org/10.1179/pom.1984.27.1.39

20. D.N. Lee, H.I. Kim, Plastic yield behaviour of porous metal. Powder. Metall. **35**(4), 275–279 (1992). https://doi.org/10.1179/pom.1992.35.4.27
21. H.C. Yang, J.W. Lee, K.T. Kim, Rubber isostatic pressing of metal powder under warm temperatures. Powder. Technol. **139**, 240–251 (2004). https://doi.org/10.1016/j.powtec.2003.01.001
22. Z.M. Lu, X.F. Gao, W.K. Zhang et al., Effect of soft-mould pressing method on anisotropy of the graphitic matrix spheres: dry-bag isostatic vs. Quasi-isostatic. J. Nucl. Mater. **570**, 153950 (2022). https://doi.org/10.1016/j.jnucmat.2022.153950
23. X.W. Zhou, Z.M. Lu, J. Zhang et al., Studies on the dimensional and mass changes of spherical fuel element during the heat treatment. Carbon Technol. **33**(6), 1–4 (2014)
24. S.P. Jing, C. Zhang, J. Pu et al., 3D microstructures of nuclear graphite: IG-110, NBG-18 and NG-CT-10. Nucl. Sci. Tech. **27**, 66 (2016). https://doi.org/10.1007/s41365-016-0071-0
25. R.E Schulze, H.A. Schulze, W. Rind, *Graphitic matrix materials for spherical HTR fuel elements*. Juel-Spe-167, Juni 1982.
26. R.R. Yang, Y. Yuan, C. Hao et al., k_{eff} uncertainty quantification and analysis due to nuclear data during the full lifetime burnup calculation for a small-sized prismatic high temperature gas-cooled reactor. Nucl. Sci. Tech. 32, 127 (2021).https://doi.org/10.1007/s41365-021-00969-w
27. H.M. Şahin, G. Tunç, A. Karakoç et al., Neutronic study on the effect of first wall material thickness on tritium production and material damage in a fusion reactor. Nucl. Sci. Tech. 33, 43 (2022). https://doi.org/10.1007/s41365-022-01029-7
28. M.L. Tan, G.F. Zhu, Z.D. Zhang et al., Burnup optimization of once-through molten salt reactors using enriched uranium and thorium. Nucl. Sci. Tech. 33, 5 (2022). https://doi.org/10.1007/s41365-022-00995-2